Effective interaction quenching in artificial kagomé spin chains

L. Salmon,[1] V. Schánilec,[1,2] J. Coraux,[1] B. Canals,[1] and N. Rougemaille[1]
[1]*Université Grenoble Alpes, CNRS, Grenoble INP, Institut NÉEL, 38000 Grenoble, France*
[2]*Central European Institute of Technology, CEITEC BUT, Brno University of Technology, Purkyňova 123, Brno 612 00, Czech Republic*

(Received 27 September 2023; revised 29 January 2024; accepted 30 January 2024; published 22 February 2024)

Achieving thermal equilibrium in two-dimensional lattices of interacting nanomagnets has been a key issue on the route to study exotic phases in artificial frustrated magnets. We revisit this issue in one-dimensional artificial kagomé spin chains. Imaging arrested microstates resulting from a field demagnetization protocol and analyzing their pairwise spin correlations in real space, we unveil a nonequilibrated physics. Remarkably, this physics can be reformulated into an at-equilibrium one by rewriting the associated spin Hamiltonian in such a way that one of the coupling constants is quenched. We interpret this quenching mechanism as a kinetic hinderance occurring upon demagnetization, which induces the formation of local flux closure spin configurations that compete with those energetically favored by the magnetostatic interaction coupling the nanomagnets.

DOI: 10.1103/PhysRevB.109.054425

I. INTRODUCTION

Arrays of interacting magnetic nanostructures are powerful experimental platforms [1–8] in which to probe and emulate a wide range of phenomena [9,10] often associated with highly frustrated magnetism [11,12]. For example, spin ice physics [13,14], and Coulomb phase properties more specifically [15,16], have become accessible to real space imaging and reciprocal space analysis using lithographically patterned arrays of nanomagnets [17–28]. Recently, other forms of thus-fabricated synthetic two-dimensional (2D) lattices have been even designed to study a whole zoology of frustrated lattice spin models [29] having no equivalent in bulk compounds [30–36].

The properties of these artificially designed systems turn out to be usually well described by a physics at thermodynamic equilibrium. In particular, all measurable quantities accessible through the imaging of spin microstates can be rationalized with on-lattice spin models thermalized at a given temperature [37–39]. The experimental challenge then lies less in the ability to thermalize the system than in the capability to access different temperatures [22,25]. This is particularly true when it comes to exploring physical phenomena that emerge at low temperatures or when approaching a phase transition [18,27,40–42].

While the vast majority of studies to date have focused on 2D arrays of various geometries, sophisticated fabrication methods are being employed to build and image three-dimensional (3D) [43–46] or quasi-3D [17,21] artificial arrays. In contrast, there are few works only on one-dimensional (1D) systems, and these works have been devoted to the physics of Ising chains with ferromagnetic [47] or antiferromagnetic [48] interactions. Interestingly, in contrast to their 2D counterparts, artificial spin chains sometimes exhibit a phase diagram richer than the one expected from their associated spin model. This is the case of Ising spin chains with antiferromagnetic interactions [48], in which metastable ordered patterns can be stabilized experimentally due to micromagnetic effects [49,50], not accounted for by a point dipole model. These effects open up new prospects for the investigation of metastable configurations and illustrate the value of comparing the thermodynamics of spin models with their experimental emulation.

Pursuing this idea, we study in this work the magnetic correlations in kagomé spin chains submitted to a field demagnetization protocol, with the aim of understanding how their physics potentially differs from that of their 2D parent lattices, for which an abundant literature exists [2–6,51–55]. Following the methodology employed previously [48], we fabricated permalloy kagomé spin chains that were demagnetized using an external applied magnetic field. The resulting spin microstates were then imaged by magnetic force microscopy. Analysis of the magnetic correlations reveals that these chains exhibit signatures of a nonequilibrated physics. In particular, one magnetic correlator differs substantially and systematically from the predicted at-equilibrium value. Remarkably, this nonequilibrated physics can be rationalized using a modified spin Hamiltonian in which a specific coupling constant is quenched. The values of the correlations obtained with this modified Hamiltonian, thermalized at a well-defined temperature, nicely agree with the experimental measurements. In other words, while the field procedure applied to our kagomé spin chains does not allow us to obtain microstates representative of configurations at thermodynamic equilibrium, an effective thermodynamics does account for the experimental data, provided that a certain coupling in the spin Hamiltonian is quenched. In this sense, artificial kagomé spin chains have a behavior upon field demagnetization that differs from that of their parent 2D lattices. However, both systems share a common property: after being field demagnetized, they remain frozen at a relatively high effective temperature, of the order of a fraction of the coupling strength between nearest neighbors. Thus, reducing the dimensionality does not appear as an efficient means to reach low-energy configurations in field-demagnetized artificial systems.

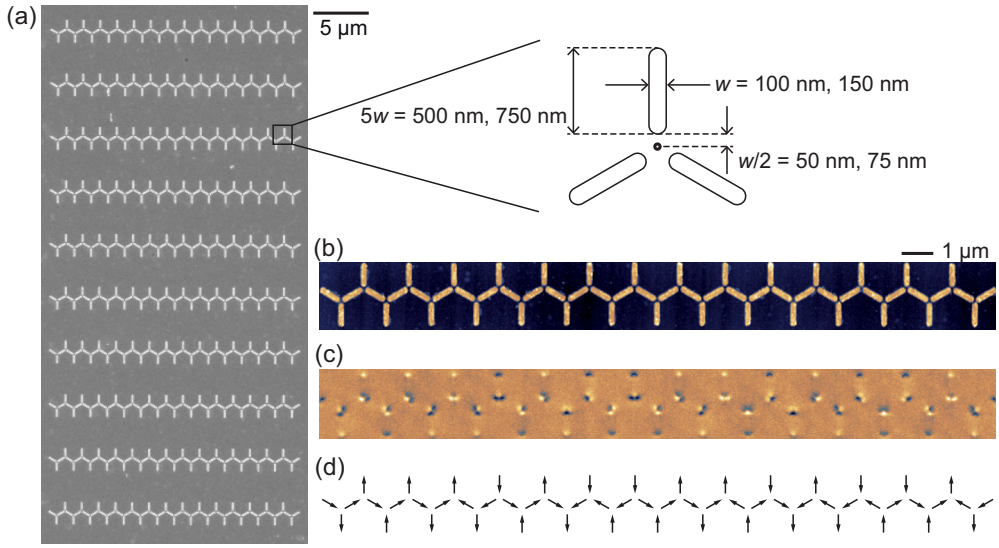

FIG. 1. (a) Scanning electron micrograph of a series of 10 kagomé spin chains and schematics illustrating the typical dimensions of the nanomagnets constituting the chains. (b) Atomic force microscopy image of an artificial kagomé spin chain. (c) Magnetic force microscopy image of the same chain after a field demagnetization protocol. The dark/bright contrasts give the magnetization direction within each nanomagnet. (d) From the magnetic image shown in (c) the spin microstate of the chain is derived.

II. EXPERIMENTAL AND THEORETICAL DETAILS

A. Sample fabrication and demagnetization

The kagomé spin chains are made of permalloy and the nanomagnets have $w \times 5w \times 30$ nm typical dimensions, with $w = 100$ or 150 nm being the width of the nanomagnets [see Fig. 1(a)]. To ensure a strong magnetostatic coupling between the elements, the distance separating the extremity of a nanomagnet from the vertex center is fixed to $w/2$. Each chain consists of $n = 29$ (resp. 40) vertices, i.e., $N = 59$ (resp. 81) nanomagnets when $w = 150$ nm (resp. 100 nm). These chains were fabricated by electron lithography (lift-off) on a Si substrate and permalloy was e-beam evaporated.

Following previous works [56–58], the sample was rotated within an external magnetic field with an oscillating and slowly decaying amplitude, and a direction within the sample plane. The applied magnetic field typically decays from ±250 mT to 0 within 80 hours, while the sample rotation frequency is of the order of 10 Hz. The resulting magnetic configurations are imaged at room temperature using a magnetic force microscope. Figures 1(b) and 1(c) show respectively a topographic and magnetic image of a kagomé chain. In the magnetic image, dark and bright contrasts indicate the north and south poles. The absence of contrast between the two extremities of the nanomagnets shows they are single domain, and their magnetic state can be approximated by an Ising variable [Fig. 1(d)].

From the imaged magnetic configurations, spin-spin correlations can be measured. Pairwise spin correlations are defined as $C_{ij} = 1/N_{ij} \sum_{i \neq j} \sigma_i \sigma_j \, \mathbf{e_i} \cdot \mathbf{e_j}$, where σ_i is an Ising variable ($\sigma_i = \pm 1$) residing on the site i defined by the local unit vector $\mathbf{e_i}$, whereas N_{ij} is the number of ij pairs [59]. The correlations between the first six neighbors were computed from the measurements (the nomenclature for these correlations is illustrated in Fig. 2: $C_{\alpha j}$ with $j = \beta, \gamma, \ldots$ corresponding to $j = i+1, i+2, \ldots$). To improve the statistics, three series of 10 kagomé chains are considered in this work, two series (series 1 and 2) for w =150 nm and one series (series 3) for $w = 100$ nm, and each series has been demagnetized twice [one series is shown in Fig. 1(a)]. Each correlation measurement is therefore the average of 20 chains consisting of 59 or 81 Ising variables.

B. Tensor matrix approach

The correlations measured experimentally are then compared to those predicted by the thermodynamics of an on-lattice Ising spin Hamiltonian $\mathcal{H}_k$, which includes dipolar spin-spin interactions up to the kth neighbors. The Hamiltonian is thus of the form $\mathcal{H}_k = \sum J_{ij} \sigma_i \sigma_j$, with J_{ij} taking $k = 1$–6 possible values (see Table I) according to the notation described in Fig. 2.

Rather than using a Monte Carlo approach to probe the thermodynamics of our spin chains, we opted for an exact resolution using the transfer matrix method. Here, we go beyond the textbook treatment known for 1D spin chains with magnetic interactions up to the third neighbor [60]. More

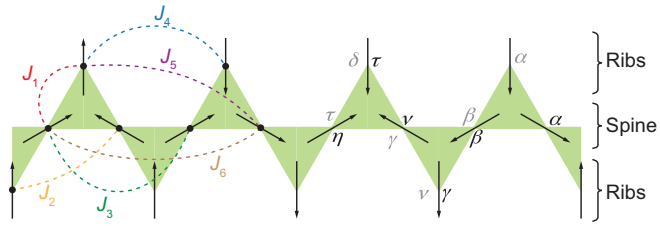

FIG. 2. Schematics of a kagomé spin chain showing the coupling strengths J_k between the kth neighbors and the notations used to identify pairwise spin correlations. The topology of the chain consists of a longitudinal spine bridging all vertices, and two transverse ribs composed of dangling spins.

TABLE I. Coupling strengths used in the dipolar spin Hamiltonian.

J_1	J_2	J_3	J_4	J_5	J_6
1	−0.137	0.045	−0.036	0.014	0.037

specifically, taking into account the coupling terms beyond the nearest neighbors requires to define spin cluster matrices having $2N \times 2N$ dimensions, where N is the number of spins comprised within the cluster. Resolution is obtained numerically and is not analytical, contrary to what was achieved for couplings up to the third neighbor [60].

III. RESULTS

The experimental measurements obtained for the three series of kagomé spin chains are reported in Table II. Several observations can be made. First, the $C_{\alpha\beta}$ correlator is always equal to 1/6, demonstrating that the ice rule is strictly obeyed (no local 3-in or 3-out configuration is observed). Second, the $C_{\alpha\gamma}$ and $C_{\alpha\delta}$ correlators are significantly negative. If this is expected from magnetostatic considerations, we note that these two correlators are substantially larger in absolute value than what is found in 2D kagomé lattices [3,6] (see Table II). This result may suggest that a field demagnetization protocol brings more efficiently 1D kagomé chains into a low-temperature regime than 2D kagomé lattices. Finally, the correlators involving the third, fifth, and sixth neighbors ($C_{\alpha\nu}$, $C_{\alpha\tau}$, and $C_{\alpha\eta}$) are lower in absolute value than the three other correlators, and their values are scattered around zero. Interestingly, these three correlators, and $C_{\alpha\nu}$ in particular, markedly differ from the values reported in 2D networks (see Table II), where they are significantly positive. The question is then why the spin model describing chains and networks differs, and whether this is a dimensionality effect.

To address this question, we first consider the spin Hamiltonian $\mathcal{H}_k$ (we recall that $k = 1$–6 is the range of the spin-spin interactions, up to the kth neighbor) described in Sec. II B. The temperature dependencies of the spin correlations deduced from the transfer matrix analysis are reported in Fig. 3(a) for the six $\mathcal{H}_k$ Hamiltonians. As expected, a nearest-neighbor description leaves the system macroscopically degenerate in its low-energy configuration, with spin correlations close to those predicted for 2D lattices [6,61]. Once the ice rule is satisfied ($C_{\alpha\beta} = 1/6$), all correlators are temperature independent. Conversely, with an interaction cutoff radius beyond nearest neighbors ($\mathcal{H}_2 \ldots \mathcal{H}_6$), ordered patterns emerge at low temperatures. The presence of longer range couplings lifts the degeneracy observed when only J_1 is considered. Remarkably, the low-temperature magnetic pattern is identical for all $\mathcal{H}_k$ ($k > 1$), with the correlators reaching the same values whatever the Hamiltonian. We note that this low-energy configuration, shown in Fig. 3(b), is the one of the (2D) dipolar kagomé spin ice [62,63].

TABLE II. Pairwise spin correlators measured for the first six neighbors in our three series of kagomé chains and from previous works on 2D kagomé lattices [59].

	$C_{\alpha\beta}$	$C_{\alpha\gamma}$	$C_{\alpha\nu}$	$C_{\alpha\delta}$	$C_{\alpha\tau}$	$C_{\alpha\eta}$
Series 1	0.167	−0.146	−0.029	−0.278	−0.005	−0.026
Series 2	0.167	−0.134	−0.004	−0.215	0.007	−0.022
Series 3	0.167	−0.117	0.035	−0.189	−0.010	0.007
2D [3]	0.167	−0.079	0.165	−0.130		
2D [6]	0.164	−0.056	0.151	−0.063	0.013	0.056

TABLE III. Pairwise spin correlators measured for the two subfamilies of the third neighbors in our three series of kagomé chains. $C'_{\alpha\nu}$ is the correlator involving dangling bonds and $C''_{\alpha\nu}$ the one involving a spin pair within the spine of the chain.

Series	$C'_{\alpha\nu}$	$C''_{\alpha\nu}$
1	0.004	−0.061
2	0.032	−0.025
3	0.062	0.008

The question that now arises is whether these models account for the experimental observations. To answer this question, it is instructive to compare the calculated temperature dependencies of the spin correlators to the values reported in Table II. Interestingly, the measurements clearly show that $C_{\alpha\delta}$ is always smaller than $C_{\alpha\gamma}$ (almost by a factor of 2), whatever the chain series we consider. These measurements are incompatible with the first three Hamiltonians $\mathcal{H}_1$, $\mathcal{H}_2$, and $\mathcal{H}_3$ [in these three cases, $C_{\alpha\gamma}$ is close, but smaller than $C_{\alpha\delta}$; see red and orange curves in the upper panels of Fig. 3(a)]. Conversely, the other three models ($\mathcal{H}_4$, $\mathcal{H}_5$, $\mathcal{H}_6$) predict $C_{\alpha\gamma}$ and $C_{\alpha\delta}$ values agreeing with the experimental ones within a certain temperature range, indicated by the gray shaded areas [see lower panels of Fig. 3(a)]. Nevertheless, within this temperature window, the agreement is poor with the other spin correlators. In particular, $C_{\alpha\nu}$ is not captured by the models [see inset in the bottom-left graph of Fig. 3(a) where the discrepancy between numerical and experimental results is reported for this correlator]. Results are similar for $C_{\alpha\eta}$ and $C_{\alpha\tau}$, whose experimental values are lower than the predicted ones, and whose sign is sometimes opposite to the expected one. These observations suggest that a nontrivial mechanism is at work in our experiment.

At this point, it is worth mentioning that the $C_{\alpha\nu}$ correlator (like $C_{\alpha\beta}$) has a specific feature compared to the other correlators: It involves a pair of spins belonging both to the spine of the chain or both to the ribs. Contrary to the other correlators, $C_{\alpha\nu}$ can thus be calculated for two distinct subsets of spin pairs [see inset of Fig. 4(a)]. Experimental measurements of the corresponding correlators, $C'_{\alpha\nu}$ (involving dangling spins) and $C''_{\alpha\nu}$ (spins within the spine), reveal a surprising result: $C'_{\alpha\nu}$ is systematically larger than $C''_{\alpha\nu}$ (see Table III). Recalling that these pairs of spins are coupled by a third-neighbor term J_3 (Fig. 2), this experimental observation questions the relevance of a single J_3 value. In the following, we define J'_3 as the coupling involving dangling spins and J''_3 involving a spin pair in the spine of the chain [see inset of Fig. 4(a)]. Since the $C_{\alpha\nu}$ correlator is smaller than the predicted value, it is reasonable to assume that J_3 is effectively smaller than what it should be. Experimentally, $C'_{\alpha\nu} > C''_{\alpha\nu}$, suggesting that J'_3 could be larger than J''_3. We emphasize that, from a dipolar point of

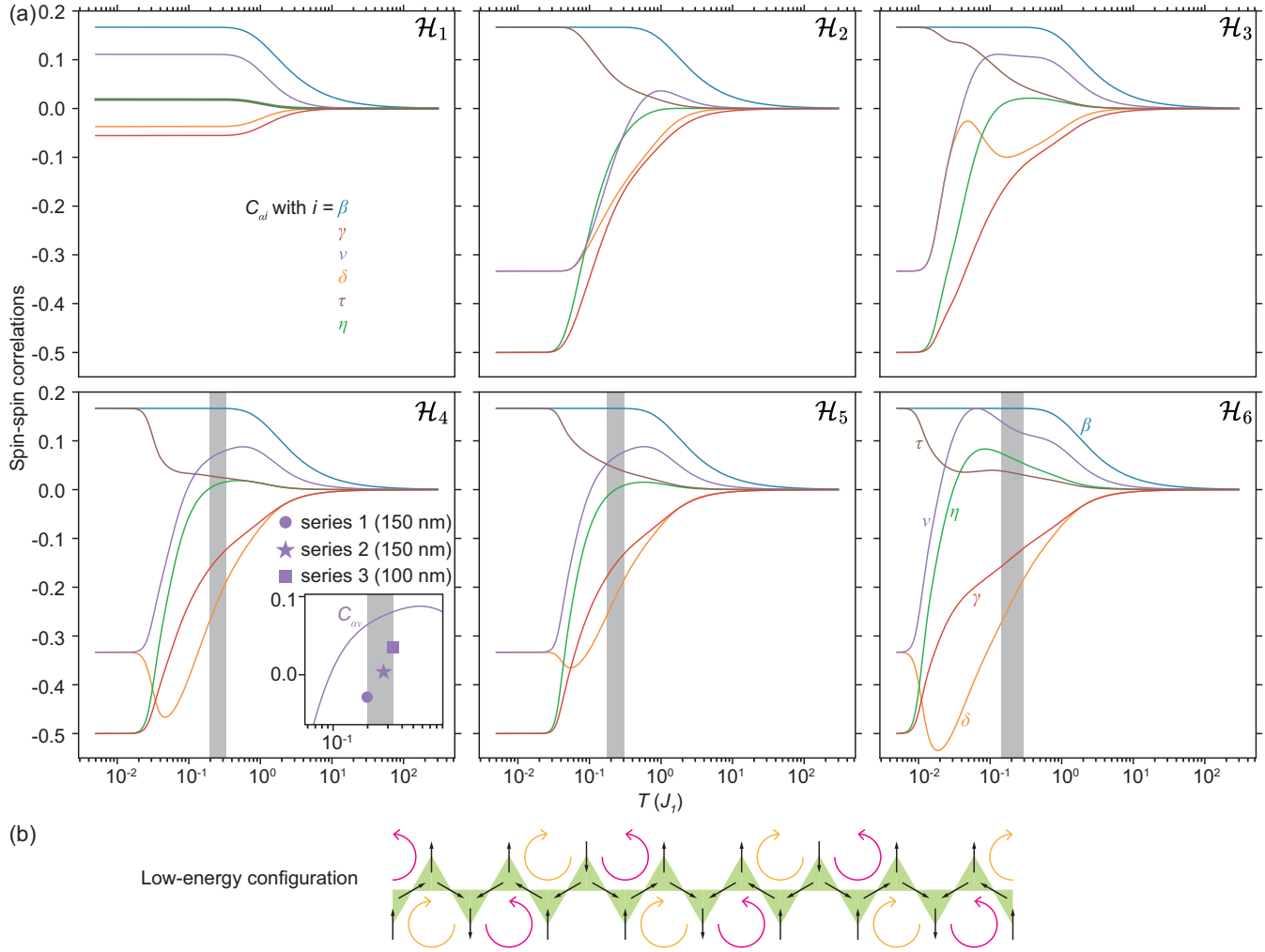

FIG. 3. (a) Temperature dependence of the magnetic correlations between the first six nearest neighbors as defined in Fig. 2. Six scenarios are considered depending on the range of the dipolar interaction. From the upper-left panel to the lower-right panel, the range of the interaction extends from the first to the sixth neighbor, as indicated by the index k in the spin Hamiltonian $\mathcal{H}_k$. The gray shaded area in the lower three panels indicates the temperature window compatible with the measured $C_{\alpha\beta}$, $C_{\alpha\gamma}$, and $C_{\alpha\delta}$ correlators. This temperature window is also compatible with the measured value of the sixth correlator $C_{\alpha\eta}$ (except for $\mathcal{H}_6$). However, it is clearly incompatible with the third and fifth correlators, and $C_{\alpha\nu}$ more specifically. This is evidenced in the inset corresponding to $\mathcal{H}_4$ where the temperature dependence of $C_{\alpha\nu}$ is shown together with the average values obtained experimentally for the three spin chains. (b) Schematics of the configuration found at low temperature in all cases but $\mathcal{H}_1$. This configuration is the ground state found in the dipolar kagomé spin ice. It is characterized by local flux closure configurations with alternating chirality represented by yellow (clockwise) and purple (anticlockwise) circular arrows (see head-to-tail arrangements of the spins along the edges of open hexagons).

view, there is however no reason to consider two distinct J_3 coupling terms, and such a distinction can only be effective.

The correlators deduced from the models studied previously (Fig. 3) were thus recalculated by imposing $J_3'' = 0$, leaving $J_3' = J_3 = 0.045$ unchanged. The choice to set $J_3'' = 0$ is simply based on the fact that J_3 is already small (see Table I), a natural smaller value being 0. Unsurprisingly, the $\mathcal{H}_1$, $\mathcal{H}_2$, and $\mathcal{H}_3$ models are still not compatible with the experimental data. However, good agreement is obtained as soon as the model includes interactions up to at least the fourth neighbor ($\mathcal{H}_4$, $\mathcal{H}_5$, and $\mathcal{H}_6$ to a lesser extent). Figure 4(a) illustrates this agreement when considering the $\mathcal{H}_4$ model. Interestingly, besides the six studied correlators, the distinction between $C'_{\alpha\nu}$ and $C''_{\alpha\nu}$ is also well described [see purple dashed curves and open symbols in Figs. 4(a) and 4(b)]. This overall agreement between experiments and numerical predictions is actually very good for both $\mathcal{H}_4$ and $\mathcal{H}_5$, but less so when J_6 is taken into account. This is again consistent with the fact that the effective coupling involving a spin pair within the spine of the chain is reduced. Indeed, J_6 being ferromagnetic (like J_3) and involving spin pairs within the spine (and only within the spine; see Fig. 2), taking it into account degrades the agreement with the experiments (we will see why in the next section). In other words, a good match is obtained when the coupling terms J_3'' and J_6, both involving spin pairs belonging to the spine of the chain, are quenched.

We emphasize that the predictions from the modified $\mathcal{H}_4$ Hamiltonian fit sufficiently well the experimental data to associate distinct effective temperatures to the three chain series. As illustrated in Fig. 4(b), the (thermal) energy of the

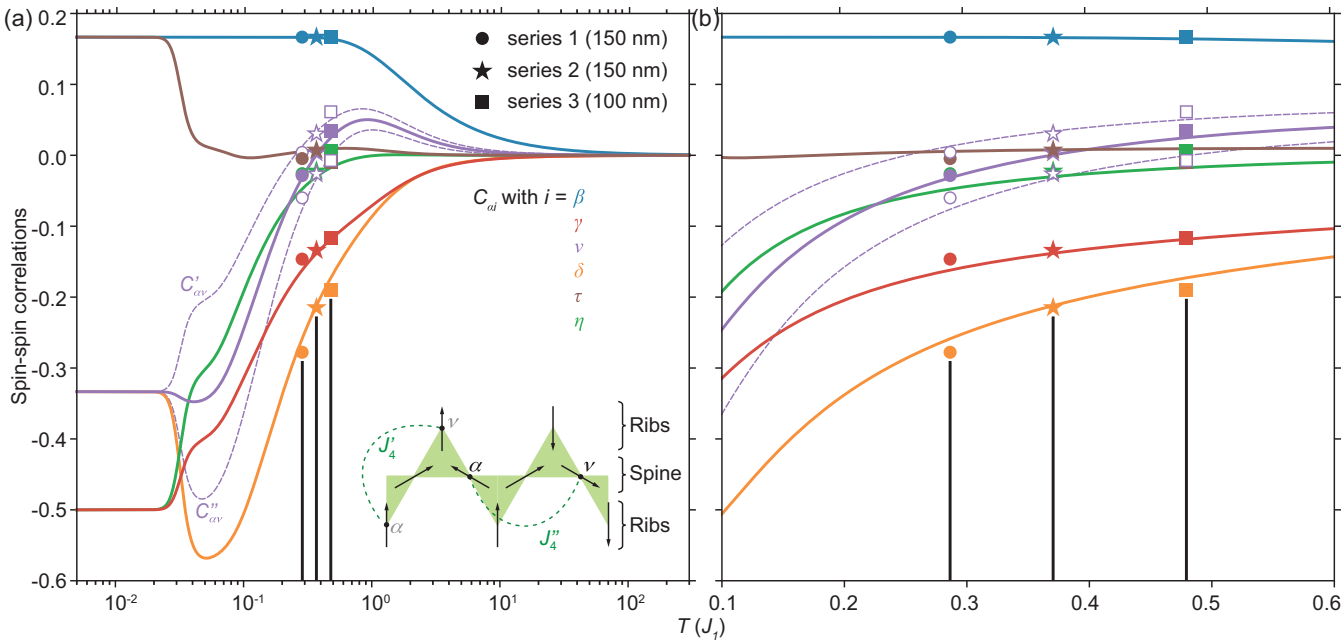

FIG. 4. (a) Temperature dependence of the magnetic correlations between the first six nearest neighbors as defined in Fig. 2 for the $\mathcal{H}_4$ spin Hamiltonian in which J_3'' is set to 0. The predictions fit well the experimental findings marked by colored dots, stars, and squares for samples 1, 2, and 3, respectively. The difference between the J_3' and J_3'' couplings is illustrated in the inset. The corresponding $C'_{\alpha\nu}$ and $C''_{\alpha\nu}$ correlators are plotted as purple dashed lines and open symbols. (b) Zoom-in of the full temperature window reported in (a).

configurations we image is typically about 1/2 or 1/3 of the J_1 energy term, meaning that our demagnetization protocol brings the kagomé spin chains into relatively low-energy configurations. We observe that the first two series (series 1 and 2) have a lower effective temperature than the third one (series 3), suggesting that wide nanomagnets are better suited for reaching low-energy configurations.

IV. INTERPRETATION

The natural question that arises is why a modified Hamiltonian, in which J_3'' is quenched, is able to account for the experimental measurements. It is striking that this is the case for three series of chains, found to be equilibrated at different effective temperatures [see Figs. 4(a) and 4(b)]. Although these effective temperatures lie in a narrow window (from $J_1/3$ to $J_1/2$ typically), some correlators ($C_{\alpha\delta}$ in particular) vary abruptly within this range, whereas others (like $C_{\alpha\tau}$) are essentially constant. The Hamiltonian in which J_3'' is quenched captures well all these temperature dependencies.

We stress again that the couplings are experimentally ruled by magnetostatics, and there is no reason why some couplings should be screened. For reasons likely originating from the demagnetization procedure, the kagomé chains are not found in configurations representative of thermodynamic equilibrium, but rather exhibit nonequilibrium behavior. The quenching of a specific coupling can only be understood in an effective manner.

Given the fact that the spin dynamics is governed experimentally by magnetization reversal processes, considering two coupling terms J_3' and J_3'' might be relevant. Indeed, a spin pair in the spine of the chain involves nanomagnets having a coordination number of 4, whereas it is 2 for spins involving dangling bonds. Since magnetization reversal is triggered at the nanomagnet extremities, we might expect that dangling spins fluctuate more on average because of their free end than spins within the spine. We could then argue that dangling spins fluctuate sufficiently to reach an equilibrated state, whereas the dynamics of the spins belonging to the spine freezes quickly, being weakly correlated, especially when the associated coupling strength is small (like J_3). More generally, we could argue that the physics of our spin chains is essentially governed by J_{ij} couplings involving at least one dangling spin (with the exception of $J_{\alpha\beta}$, for which the interaction is very strong due to the small distance between the extremities of neighboring nanomagnets). Since only J_3'' and J_6 couple spins all belonging to the spine of the chain, these two couplings could be effectively quenched because of the intrinsic field-induced magnetization dynamics within the chains.

We may also argue that the demagnetization procedure favors the formation of local flux-closure configurations. Indeed, the spin microstates we image clearly reveal local windings, sometimes over several successive open hexagons. This effect is illustrated in Fig. 5 for four chains in which local flux closure configurations are indicated by yellow and pink oriented loops. Importantly, the formation of these local loops imposes a negative $C_{\alpha\nu}$ correlation along the spine (antiparallel spins), competing with the positive correlations expected from the magnetostatic interaction. We note that the formation of such local loops is compatible with the argument above suggesting that dangling spins fluctuate more than spins within the spine of the chain. In fact, these two effects could be intimately related, explaining why J_3'' is effectively quenched.

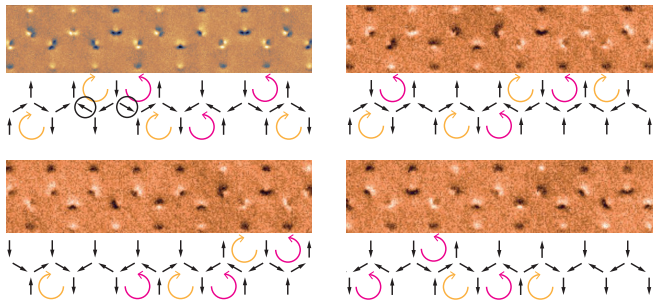

FIG. 5. Experimental magnetic images and their corresponding spin states for four different kagomé spin chains. Each chain is characterized by several local flux closure configurations represented by clockwise (yellow) and anticlockwise (purple) circular arrows. Successive yellow/purple loops impose an antiferromagnetic alignment of $\alpha\nu$ (and $\alpha\eta$) spin pairs belonging to the spine of the chain (two of such $\alpha\nu$ spins are marked by a black circle).

V. CONCLUSION

In this work, we have investigated experimentally the magnetic correlations that develop in field-demagnetized artificial kagomé spin chains. The central result is the observation of a specific pairwise spin correlator whose value substantially and reproducibly deviates from the one expected at thermodynamic equilibrium. This suggests that an out-of-equilibrium physics is at play in our experiment, and like antiferromagnetically coupled Ising chains [48], the arrested microstates we imaged are not accounted for by a canonical spin Hamiltonian. However, whereas a metastable ordered pattern emerges in antiferromagnetic Ising chains [48], the kagomé spin chains remain disordered. In both types of chains, unpredicted configurations can be reached after a field demagnetization protocol, opening new prospects to access metastable and/or unusual correlations in artificial spin systems.

As a natural extension of our work, we could now investigate how the field demagnetization protocol itself impacts the properties of the resulting magnetic microstates. Since metastable configurations are obtained with a slowly decaying and oscillating magnetic field, we might wonder whether other metastable states could be stabilized by ramping down the field differently. This could be done for example with a simple linear decay of the field amplitude [58], using the same protocol with various field step sizes [56,57] or without rotating the sample to demagnetize the lattice in one direction only. Here, the strategy we followed is the one we have employed in several other studies that have revealed that equilibrated low-energy configurations could be reached successfully and reproducibly, regardless of the system geometry [6,8,17,22,23,25]. Using this previously benchmarked field protocol then allows direct comparison with previous works, especially with what has been observed in antiferromagnetic Ising chains [48]. In addition, investigating thermally active kagomé spin chains would be of particular interest to understand to what extent the metastable states we imaged are linked to the presence of an applied magnetic field.

Finally, our results demonstrate that the physics of artificial spin structures is long-ranged, and a short-range spin Hamiltonian clearly fails to capture the experimental findings. Our correlation analysis indicates that it is reasonable to consider that the effective cutoff radius of the magnetostatic interaction extends up to the fourth/fifth neighbors at least, consistent with what is found in 2D lattices [6,23]. Our measurements also suggest that the physics of small-size 2D kagomé spin ice might be affected by the presence of dangling spins at the lattice edges. As a result, magnetic correlations might be different in the bulk of the system and at the vicinity of the lattice edges. To what extent such effects could impact the physics in 2D networks remains an open question.

ACKNOWLEDGMENTS

The authors warmly thank Yann Perrin and Van-Dai Nguyen for providing technical help in the fabrication and characterization of the sample.

[1] R. F. Wang, C. Nisoli, R. S. Freitas, J. Li, W. McConville, B. J. Cooley, M. S. Lund, N. Samarth, C. Leighton, V. H. Crespi, and P. Schiffer, Nature (London) **439**, 303 (2006).
[2] M. Tanaka, E. Saitoh, H. Miyajima, T. Yamaoka, and Y. Iye, Phys. Rev. B **73**, 052411 (2006).
[3] Y. Qi, T. Brintlinger, and J. Cumings, Phys. Rev. B **77**, 094418 (2008).
[4] S. Ladak, D. E. Read, G. K. Perkins, L. F. Cohen, and W. R. Branford, Nat. Phys. **6**, 359 (2010).
[5] E. Mengotti, L. J. Heyderman, A. Fraile Rodríguez, F. Nolting, R. V. Hügli, and H.-B. Braun, Nat. Phys. **7**, 68 (2011).
[6] N. Rougemaille, F. Montaigne, B. Canals, A. Duluard, D. Lacour, M. Hehn, R. Belkhou, O. Fruchart, S. El Moussaoui, A. Bendounan, and F. Maccherozzi, Phys. Rev. Lett. **106**, 057209 (2011).
[7] S. Zhang, J. Li, I. Gilbert, J. Bartell, M. J. Erickson, Y. Pan, P. E. Lammert, C. Nisoli, K. K. Kohli, R. Misra, V. H. Crespi, N. Samarth, C. Leighton, and P. Schiffer, Phys. Rev. Lett. **109**, 087201 (2012).
[8] I. A. Chioar, N. Rougemaille, A. Grimm, O. Fruchart, E. Wagner, M. Hehn, D. Lacour, F. Montaigne, and B. Canals, Phys. Rev. B **90**, 064411 (2014).
[9] C. Nisoli, R. Moessner, and P. Schiffer, Rev. Mod. Phys. **85**, 1473 (2013).
[10] N. Rougemaille and B. Canals, Eur. Phys. J. B **92**, 62 (2019).
[11] C. Lacroix, P. Mendels, and F. Mila (eds.), *Introduction to Frustrated Magnetism: Materials, Experiments, Theory* (Springer, Berlin, Heidelberg, 2011).
[12] H. T. Diep (ed.), *Frustrated Spin Systems* (World Scientific Publishing, Singapore, 2013).
[13] M. J. Harris, S. T. Bramwell, D. F. McMorrow, T. Zeiske, and K. W. Godfrey, Phys. Rev. Lett. **79**, 2554 (1997).
[14] S. T. Bramwell and M. J. Harris, J. Phys.: Condens. Matter **32**, 374010 (2020).

[15] C. L. Henley, Annu. Rev. Condens. Matter Phys. **1**, 179 (2010).
[16] J. Rehn and R. Moessner, Philos. Trans. R. Soc. A **374**, 20160093 (2016).
[17] Y. Perrin, B. Canals, and N. Rougemaille, Nature (London) **540**, 410 (2016).
[18] O. Sendetskyi, L. Anghinolfi, V. Scagnoli, G. Möller, N. Leo, A. Alberca, J. Kohlbrecher, J. Luning, U. Staub, and L. J. Heyderman, Phys. Rev. B **93**, 224413 (2016).
[19] B. Canals, I.-A. Chioar, V.-D. Nguyen, M. Hehn, D. Lacour, F. Montaigne, A. Locatelli, T. O. Menteş, B. Santos Burgos, and N. Rougemaille, Nat. Commun. **7**, 11446 (2016).
[20] E. Östman, H. Stopfel, I.-A. Chioar, U. B. Arnalds, A. Stein, V. Kapaklis, and B. Hjörvarsson, Nat. Phys. **14**, 375 (2018).
[21] A. Farhan, M. Saccone, C. F. Petersen, S. Dhuey, R. V. Chopdekar, Y.-L. Huang, N. Kent, Z. Chen, M. J. Alava, T. Lippert, A. Scholl, and S. van Dijken, Sci. Adv. **5**, eaav6380 (2019).
[22] V. Schánilec, B. Canals, V. Uhlíř, L. Flajšman, J. Sadílek, T. Šikola, and N. Rougemaille, Phys. Rev. Lett. **125**, 057203 (2020).
[23] O. Brunn, Y. Perrin, B. Canals, and N. Rougemaille, Phys. Rev. B **103**, 094405 (2021).
[24] N. Rougemaille and B. Canals, Appl. Phys. Lett. **118**, 112403 (2021).
[25] V. Schánilec, O. Brunn, M. Horáček, S. Krátký, P. Meluzín, T. Šikola, B. Canals, and N. Rougemaille, Phys. Rev. Lett. **129**, 027202 (2022).
[26] W.-C. Yue, Z. Yuan, Y.-Y. Lyu, S. Dong, J. Zhou, Z.-L. Xiao, L. He, X. Tu, Y. Dong, H. Wang, W. Xu, L. Kang, P. Wu, C. Nisoli, W.-K. Kwok, and Y.-L. Wang, Phys. Rev. Lett. **129**, 057202 (2022).
[27] K. Hofhuis, S. H. Skjærvø, S. Parchenko, H. Arava, Z. Luo, A. Kleibert, P. M. Derlet, and L. J. Heyderman, Nat. Phys. **18**, 699 (2022).
[28] Y. Perrin, B. Canals, and N. Rougemaille, Phys. Rev. B **99**, 224434 (2019).
[29] S. H. Skjærvø, C. H. Marrows, R. L. Stamps, and L. J. Heyderman, Nat. Rev. Phys. **2**, 13 (2020).
[30] I. Gilbert, G.-W. Chern, S. Zhang, L. O'Brien, B. Fore, C. Nisoli, and P. Schiffer, Nat. Phys. **10**, 670 (2014).
[31] I. Gilbert, Y. Lao, I. Carrasquillo, L. O'Brien, J. D. Watts, M. Manno, C. Leighton, A. Scholl, C. Nisoli, and P. Schiffer, Nat. Phys. **12**, 162 (2016).
[32] A. Farhan, C. F. Petersen, S. Dhuey, L. Anghinolfi, Q. H. Qin, M. Saccone, S. Velten, C. Wuth, S. Gliga, P. Mellado, M. J. Alava, A. Scholl, and S. van Dijken, Nat. Commun. **8**, 995 (2017).
[33] D. Louis, D. Lacour, M. Hehn, V. Lomakin, T. Hauet, and F. Montaigne, Nat. Mater. **17**, 1076 (2018).
[34] D. Shi, Z. Budrikis, A. Stein, S. A. Morley, P. D. Olmsted, G. Burnell, and C. H. Marrows, Nat. Phys. **14**, 309 (2018).
[35] N. Leo, S. Holenstein, D. Schildknecht, O. Sendetskyi, H. Luetkens, P. M. Derlet, V. Scagnoli, D. Lanon, J. R. L. Mardegan, T. Prokscha, A. Suter, Z. Salman, S. Lee, and L. J. Heyderman, Nat. Commun. **9**, 2850 (2018).
[36] X. Zhang, A. Duzgun, Y. Lao, S. Subzwari, N. S. Bingham, J. Sklenar, H. Saglam, J. Ramberger, J. T. Batley, J. D. Watts, D. Bromley, R. V. Chopdekar, L. O'Brien, C. Leighton, C. Nisoli, and P. Schiffer, Nat. Commun. **12**, 6514 (2021).
[37] C. Nisoli, R. Wang, J. Li, W. F. McConville, P. E. Lammert, P. Schiffer, and V. H. Crespi, Phys. Rev. Lett. **98**, 217203 (2007).
[38] C. Nisoli, J. Li, X. Ke, D. Garand, P. Schiffer, and V. H. Crespi, Phys. Rev. Lett. **105**, 047205 (2010).
[39] I. A. Chioar, B. Canals, D. Lacour, M. Hehn, B. Santos Burgos, T. O. Menteş, A. Locatelli, F. Montaigne, and N. Rougemaille, Phys. Rev. B **90**, 220407(R) (2014).
[40] A. Farhan, P. M. Derlet, A. Kleibert, A. Balan, R. V. Chopdekar, M. Wyss, L. Anghinolfi, F. Nolting, and L. J. Heyderman, Nat. Phys. **9**, 375 (2013).
[41] L. Anghinolfi, H. Luetkens, J. Perron, M. G. Flokstra, O. Sendetskyi, A. Suter, T. Prokscha, P. M. Derlet, S. L. Lee, and L. J. Heyderman, Nat. Commun. **6**, 8278 (2015).
[42] O. Sendetskyi, V. Scagnoli, N. Leo, L. Anghinolfi, A. Alberca, J. Lüning, U. Staub, P. M. Derlet, and L. J. Heyderman, Phys. Rev. B **99**, 214430 (2019).
[43] A. May, M. Hunt, A. van den Berg, A. Hejazi, and S. Ladak, Commun. Phys. **2**, 13 (2019).
[44] J. Llandro, D. M. Love, A. Kovács, J. Caron, K. N. Vyas, A. Kákay, R. Salikhov, K. Lenz, J. Fassbender, M. R. J. Scherer, C. Cimorra, U. Steiner, C. H. W. Barnes, R. E. Dunin-Borkowski, S. Fukami, and H. Ohno, Nano Lett. **20**, 3642 (2020).
[45] A. May, M. Saccone, A. van den Berg, J. Askey, M. Hunt, and S. Ladak, Nat. Commun. **12**, 3217 (2021).
[46] M. Saccone, A. Van den Berg, E. Harding, S. Singh, S. R. Giblin, F. Flicker, and S. Ladak, Commun. Phys. **6**, 217 (2023).
[47] E. Östman, U. B. Arnalds, V. Kapaklis, A. Taroni, and B. Hjörvarsson, J. Phys.: Condens. Matter **30**, 365301 (2018).
[48] V.-D. Nguyen, Y. Perrin, S. Le Denmat, B. Canals, and N. Rougemaille, Phys. Rev. B **96**, 014402 (2017).
[49] N. Rougemaille, F. Montaigne, B. Canals, M. Hehn, H. Riahi, D. Lacour, and J.-C. Toussaint, New J. Phys. **15**, 035026 (2013).
[50] K. Zeissler, S. K. Walton, S. Ladak, D. E. Read, T. Tyliszczak, L. F. Cohen, and W. R. Branford, Sci. Rep. **3**, 1252 (2013).
[51] S. Zhang, I. Gilbert, C. Nisoli, G.-W. Chern, M. J. Erickson, L. O'Brien, C. Leighton, P. E. Lammert, V. H. Crespi, and P. Schiffer, Nature (London) **500**, 553 (2013).
[52] F. Montaigne, D. Lacour, I. A. Chioar, N. Rougemaille, D. Louis, S. Mc Murtry, H. Riahi, B. Santos Burgos, T. O. Menteş, A. Locatelli, B. Canals, and M. Hehn, Sci. Rep. **4**, 5702 (2014).
[53] A. Farhan, P. M. Derlet, L. Anghinolfi, A. Kleibert, and L. J. Heyderman, Phys. Rev. B **96**, 064409 (2017).
[54] D. Sanz-Hernández, M. Massouras, N. Reyren, N. Rougemaille, V. Schánilec, K. Bouzehouane, M. Hehn, B. Canals, D. Querlioz, J. Grollier, F. Montaigne, and D. Lacour, Adv. Mater. **33**, 2008135 (2021).
[55] K. Hofhuis, A. Hrabec, H. Arava, N. Leo, Y.-L. Huang, R. V. Chopdekar, S. Parchenko, A. Kleibert, S. Koraltan, C. Abert, C. Vogler, D. Suess, P. M. Derlet, and L. J. Heyderman, Phys. Rev. B **102**, 180405(R) (2020).
[56] R. F. Wang, J. Li, W. McConville, C. Nisoli, X. Ke, J. W. Freeland, V. Rose, M. Grimsditch, P. Lammert, V. H. Crespi, and P. Schiffer, J. Appl. Phys. **101**, 09J104 (2007).
[57] X. Ke, J. Li, C. Nisoli, Paul E. Lammert, W. McConville, R. F. Wang, V. H. Crespi, and P. Schiffer, Phys. Rev. Lett. **101**, 037205 (2008).
[58] J. P. Morgan, A. Bellew, A. Stein, S. Langridge, and C. H. Marrows, Front. Physics **1**, 28 (2013).

[59] We use the conventional definition of the magnetic correlations C_{ij} between the magnetic moments $\vec{S}_i$ and $\vec{S}_j$: $C_{ij} = \langle \vec{S}_i \cdot \vec{S}_j \rangle - \langle \vec{S}_i \rangle \langle \vec{S}_j \rangle$. In our system, the magnetic moment is an Ising variable such that $\vec{S}_i = \sigma_i \vec{e}_i$, with $\sigma_i = \pm 1$ and $\vec{e}_i$ a unit vector defining the local anisotropy axis. As a convention for the kagomé lattice, we consider unit vectors pointing outward (inward) from a $\bigtriangledown$-type ($\bigtriangleup$-type) triangle. Consequently, $\vec{e}_i \cdot \vec{e}_j = -1/2$, and $C_{ij} = -\langle \sigma_i \sigma_j \rangle / 2$. Experimentally, $\langle\ \rangle$ denotes the statistical average performed over all kagomé chains of a given series. We emphasize that other definitions could be used, explaining why different values can be found in previous literature. For example, we could omit the geometrical parameter $\vec{e}_i \cdot \vec{e}_j$, thus leading to $C_{ij} = \langle \sigma_i \sigma_j \rangle$. In other works, C_{ij} is set to +1 if $\vec{S}_i \cdot \vec{S}_j > 0$ and -1 otherwise. This is the reason why the kagomé ice-rule constraint is strictly obeyed whenever $C_{\alpha\beta} = 1/6$, $-1/3$, or $+1/3$ depending on the definition. Note that the choice of the definition may also affect other correlation values, and not only $C_{\alpha\beta}$. When we compare our values to those from other works (such as those from Ref. [3] and reported in Table I), we have of course applied a unique definition for the correlations.

[60] A. V. Zarubin, F. A. Kassan-Ogly, and A. I. Proshkin, J. Magn. Magn. Mater. **514**, 167144 (2020).

[61] A. S. Wills, R. Ballou, and C. Lacroix, Phys. Rev. B **66**, 144407 (2002).

[62] G. Möller and R. Moessner, Phys. Rev. B **80**, 140409(R) (2009).

[63] G.-W. Chern, P. Mellado, and O. Tchernyshyov, Phys. Rev. Lett. **106**, 207202 (2011).